Integrative Biology

Cite this: *Integr. Biol.*, 2011, **3**, 1102–1111

www.rsc.org/ibiology

PAPER

Engineering 3D cell instructive microenvironments by rational assembly of artificial extracellular matrices and cell patterning†

Ana Sala,[ab] Patrick Hänseler,[a] Adrian Ranga,[c] Matthias P. Lutolf,[c] Janos Vörös,[b] Martin Ehrbar*[ad] and Franz E. Weber*[a]

Received 17th May 2011, Accepted 4th September 2011
DOI: 10.1039/c1ib00045d

Engineered artificial microenvironments hold enormous potential as models to study developmental, physiological, pathological, and regenerative processes under highly defined conditions. Such platforms aim at bridging the gap between traditional *in vitro* 2D culture systems and animal models. By dissecting the biological complexity into an amenable number of parameters, systemic manipulation and study in controllable environments closely resembling the *in vivo* situation is possible. Novel strategies that address the evaluation of either ECM components, growth factors or cell–cell interactions on cellular behaviour are being developed. However, reliable methods that simultaneously recapitulate the natural instructive microenvironments in terms of cell and matrix composition, biological cues, heterogeneity and geometry are not yet available. Such spatially-defined microenvironments may be necessary to initiate and guide the formation of artificial tissues by morphogenetic processes. In this work, we introduce a flexible strategy that relies on the combination of artificial extracellular matrices with patterning techniques as well as a layer-by-layer approach to mimic rationally-designed instructive milieus. By a rational arrangement of cells and defined biochemical and biophysical extracellular cues, we report control of cell migration and generation of an artificial vascularized bone tissue-like construct.

Introduction

Traditionally, tissue engineering has aimed at the creation of functional three-dimensional (3D) tissues for therapeutic applications such as the replacement of damaged tissues. While important new mechanical and structural features for scaffolds and tissue analogs are continuously being explored, our understanding of biological and physical cues, as well as their spatiotemporal coordination during tissue regeneration is limited and consequently restricts the engineering of functional tissues based on rational design principles.[1,2] To gain insight into biological processes from *in vitro* approaches, the recapitulation of cellular microenvironments may therefore be critical.[3–6]

In vivo, tissues are characterized by complex 3D architectures with a hierarchical and heterogeneous distribution of cells and extracellular matrix (ECM) components. The local microenvironment that surrounds cells is mainly composed of the ECM, neighboring cells, soluble as well as immobilized factors, and mechanical forces. The integration of these components results in spatiotemporal and tightly controlled biochemical and biophysical arrays of signals that will determine the dynamic behavior of the cells. Thus, active microenvironments provide cells with the required information fundamental for tissue formation, homeostasis and regeneration.[7–10]

The virtual deconstruction of natural ECM components into functional subunits has inspired the engineering of artificial ECM (aECM), whose mechanical properties and biological functions can be precisely tailored.[11–17] Efforts in this field are now focused on the spatial and dynamic arrangement of biological function in 3D.[18–21] In addition, a variety of 2D cell patterning techniques, such as bioprinting,[22–26] electrophoretic patterning[27] and others,[25,28–34] have been adapted in

[a] *Department of Cranio Maxillofacial Surgery, Oral Biotechnology & Bioengineering, University Hospital Zurich and Center of Dental Medicine, University of Zurich Frauenklinikstrasse 24, Nord2 B-843, 8091 Zurich, Switzerland. E-mail: Franz.Weber@zzm.uzh.ch, Martin.Ehrbar@usz.ch; Fax: +41 44 255 4179, 044 255 44 30; Tel: +41(0)442555055, +41(0)442558513*
[b] *Institute for Biomedical Engineering, Laboratory of Biosensors and Bioelectronics, ETH Zürich, ETZ F 82, Gloriastrasse 35, 8092 Zürich, Switzerland*
[c] *Laboratory of Stem Cell Bioengineering, EPFL-SV-IBI–LSCB, Station 15, Bld AI 1109, 1015, EPF Lausanne, Switzerland*
[d] *Clinic of Obstetrics, University Hospital Zurich, Frauenklinikstrasse 24, 8091 Zurich, Switzerland*

† Electronic supplementary information (ESI) available: Four supplementary figures: (1) spreading of MC3T3-E1 on RGD-modified PEG hydrogels; (2) adhesion and spreading of C2C12 cells on RGD-modified PEG hydrogels; (3) robotic pipetting; (4) correlation between osteogenic differentiation and medium culture conditions; and two supplementary videos (360° rotating videos of spotted arrays). See DOI: 10.1039/c1ib00045d

an attempt to recapitulate the architecture of living tissues by building up 3D structures in a layer-by-layer fashion. Together, these platforms are of great value to deconstruct the *in vivo* complexity into single events and to combine them *in vitro* into instructive microenvironments and tissue-like models.

To initiate and guide the formation of artificial tissues, microenvironments consisting of spatially-defined arrangement of different cellular entities, growth factors and matrix components are likely necessary. Thus, we aimed at generating guiding microenvironments that can be systematically modified and increased in complexity, in a controllable manner, in terms of cellular, biochemical and biophysical properties as well as in their three-dimensional spatial distribution.

Here, we demonstrate that 3D heterogeneous constructs with design and organizational complexity can be engineered towards specific biological applications by combining three different technological platforms: artificial ECM (aECM) engineering, robotic printing, and layer-by-layer deposition. We recapitulate many of the features known to be important in natural milieus (ECM, neighbouring cells, soluble factors and immobilized ligands, matrix degradability and 3D spatial distribution and heterogeneity). By addressing the effect of matrix stiffness and susceptibility towards matrix degradation on cell spreading, we show that it is possible to rationally design an environment to specifically direct and control cellular spreading. By systematic evaluation of single biological constituents (RGD, VEGF, mono-, co- and tri-cultures), we demonstrate that the presence of both stromal cells, besides the adhesion ligand RGD and the pro-angiogenic growth factor VEGF, appears to be critical for endothelial cells (ECs) to form tube-like structures in artificial environments. The relevance of instructive microenvironments for the formation of functional tissue-like constructs is confirmed by the formation of organized bone tissue-like constructs that form vessel-like structures *in vitro* culture.

Materials and methods

PEG and peptides

PEG-VS and PEG-acrylate were functionalized with Lys and TG substrates (each substrate containing a cysteine) *via* the Michel-type addition to give PEG-TG, PEG-acryl-TG and PEG-MMP-Lys, PEG-acryl-MMP-Lys precursors. Functionalization and characterization of these precursors were performed as described in the existing literature.[14,15]

Formation of PEG-based hydrogels

Hydrogel networks were formed by factor XIIIa cross-linking of 8-arm PEG-TG with 8-arm PEG-MMP-Lys or 8-arm PEG-acryl-TG with 8-arm PEG-MMP-Lys as previously described.[14,15] Briefly, the covalent cross-linking of stoichiometrically balanced 8-arm PEG macromers (PEG-Lys and PEG-TG; desired PEG%) in tris buffer saline (50 mM, pH 7.6) was performed by addition of 10 U ml^{-1} of thrombin-activated factor XIIIa in the presence of 50 mM calcium chloride. The gelation occurred within a few minutes at 37 °C in a humidified incubator but the cross-linking reaction was allowed to proceed for 30 min.

Activation of FXIII by thrombin

100 μl of FXIII (200 U ml^{-1}, Fibrogammin P1250 CSL Behring) were activated in the presence of 2.5 mM $CaCl_2$ with 10 μl of thrombin (20 U ml^{-1}, Sigma-Aldrich, CH) for 30 min at 37 °C. Small aliquots (200 U ml^{-1}) of activated FXIIIa were stored at −80 °C for further use.[14,15]

Cell culture

C2C12 mesenchymal progenitor cells, MC3T3-E1 mouse preosteoblastic cells, HUVECs and MLO-osteocyte-like cell line from mouse were grown in their corresponding standard medium. MLO cells were cultured on rat tail type I collagen-coated tissue culture flasks (Becton Dickinson, FR). The cultures were never allowed to become confluent. The cells were trypsinized and passaged every 2–3 days. All cells were grown at 37 °C and 5% CO_2 in a humidified atmosphere.

Screening of medium composition for co-cultures

A screening of different mediums was performed on 2D and 3D monocultures of MC3T3-E1, MLO and HUVEC cells. Cells were grown in their standard culture medium for at least 12 hours before their medium was exchanged. Subsequently, cellular viability and morphology were assessed microscopically. In the case of preosteoblastic MC3T3-E1 cells, ALP activity without treatment or upon treatment with rhBMP-2 was quantified for each condition.

Insight, innovation, integration

The structured microenvironment that surrounds cells provides the required information fundamental for tissue formation, homeostasis and regeneration. Its misregulation leads to tissue malfunction and disease. To better understand such biological processes, reductionistic *in vitro* models that recapitulate the natural milieu while allowing for systematic evaluation from single to combinatorial biological events are needed. We describe a strategy based on artificial extracellular matrices, patterning techniques and additive layering to engineer organized instructive microenvironments which recapitulate main features of the natural milieu; extracellular matrix components, neighbouring cells, soluble as well as immobilized factors and mechanical components. By systematic evaluation we demonstrate the feasibility of engineering instructive environments to specifically direct cellular migration and to generate organized vascularized bone tissue-like constructs.

Assay of ALP activity

Medium was removed, cells were washed twice with PBS and samples were incubated for 1 hour in lysis buffer. Subsequently, equal volumes of cell lysate and ALP substrate solution were incubated for 10 min at 37 °C. The enzymatic reaction was stopped with NaOH (1 M) and, after centrifugation, the optical absorbance at 410 nm was determined.

Fabrication of PDMS films

Prepared PDMS solution was degassed in a vacuum desiccator, introduced into master molds and baked for 2 h at 60 °C. Once cured, PDMS replicas were carefully peeled off.

Additive layering protocol to form 3D assemblies

The first layer of hydrogel was cast in a mold consisting of a glass slide, a PDMS frame shaped spacer and a Sigmacote-treated glass cover. The glass cover was carefully removed after crosslinking and the cells were seeded or spotted. Subsequently, PDMS spacers of the same shape were aligned and hydrogels were formed by the same sandwich strategy. The process was consecutively repeated.

Spotting protocol

Sequential spotting was performed using standard protein and DNA printing protocol adapted to our application. Gel precursors were prepared individually and were transferred to a 4 °C reservoir immediately after addition of FXIIIa to prevent evaporation. Between spotting steps, the pin and ring were rinsed to prevent cross contamination.

Assembly of 3D bone tissue-like constructs

First, a supportive layer of 4% PEG hydrogel containing 200 μM RGD was formed on a glass slide, then MC3T3-E1 cells were seeded onto the gel, at a cell density of 2×10^5 cells cm^{-2}, and allowed to adhere for 4 hours. Subsequently, 1-μl-sized droplets of hydrolytically and proteolytically degradable PEG-acrylate gels containing single dispersed HUVEC cells (2×10^7 cells ml^{-1}) were placed on the top of the preosteoblastic monolayer. As these gels were designed to rapidly degrade, they were formed without RGD to prevent the release of large amounts of soluble RGD. Immediately after gelation the whole construct was covered with a 1.5% PEG hydrogel containing 50 μM RGD and 3×10^6 MLO cells ml^{-1}. Assemblies were cultured for 10 days or one month at 37 °C in humidified air mixed with 5% CO_2 under the standardized culture conditions in the presence (or absence) of VEGF (100 ng ml^{-1}).

Fixation and staining protocol

All constructs were fixed in 3% PBS-buffered paraformaldehyde (PFA), permeabilized with 0.5% Triton X-100 in PBS and blocked with 1% BSA and 0.5% goat serum. Subsequently, samples were incubated with primary antibodies against human CD31 or mouse bone specific ALP at 4 °C. The first antibody was detected by a Cy5-conjugated goat anti-mouse IgG (H + L) secondary antibody. F-actin staining was performed with either Alexa Fluor 546 phalloidin or Alexa Fluor 633 phalloidin and cell nuclei were detected with DAPI. Sample evaluation was performed by either confocal laser scanning microscopy or epifluorescence microscopy (Leica). Three-dimensional sampling reconstruction of the confocal *z*-stacks was performed with the Imaris software.

Measurement of tube length

The artificial tissue constructs were allowed to grow 10 days prior to fixation and staining of CD31, actin fibres and nuclei. After imaging with an epifluorescence microscope, projections of CD31 images were thresholded using Image J software and the total tubule length was traced and measured using Angio-Quant Software. The data were normalized to the evaluated area and to the control sample (single dispersed HUVECs, in the presence of RGD and VEGF/area).

Statistical analysis

Multiple comparisons were performed with Dunn's test, a nonparametric rank sum test which generalizes the Bonferroni adjustment procedure.

Results and discussion

Synthetic PEG-based hydrogels for 2D and 3D cell culture

We have previously reported a fully defined synthetic PEG-based hydrogel whose physicochemical characteristics and sensitivity to MMP proteolytic degradation can be modulated, and where growth factors or other biologically active motifs can be covalently tethered without compromising their biological activity.[14,15] The covalent cross-linking of stoichiometrically balanced 8-arm PEG macromers which are either functionalized with glutamine acceptor peptides (H-NQEQVSPL, referred to as the TG domain)[35] or lysine donor peptides (Ac-FKGG referred to as the Lys domain)[36] is catalyzed by FXIIIa transglutaminase. Simultaneous to this gelation process, cells can be encapsulated and ligands site-specifically incorporated[37] (Fig. 1a). In such conditions, human umbilical vein endothelial cells (HUVEC) and fibroblasts seeded on 5% (w/v) PEG hydrogels which contained 100 μM RGD showed, after 4 hours, comparable spreading and cytoskeleton organization as on tissue culture plastic substrates (TCP).[14,15]

In this work, we evaluate the adhesion and spreading conditions for MC3T3-E1 mouse preosteoblastic cells (Fig. S1, ESI†) and C2C12 mouse mesenchymal progenitor cells (Fig. S2, ESI†). Cells were seeded on 2D hydrogels containing different concentrations of Lys-RGD (from 0 μM to 200 μM). The optimal properties of MC3T3-E1 cells were similar to the ones previously observed for fibroblasts and HUVECs (100 μM),[14,15] whereas C2C12 cells required higher concentrations of RGD (200 μM) to reach morphologies comparable to control samples. Furthermore, the effect of matrix stiffness [from $G' \approx 250$ Pa (2% PEG) to $G' \approx 1.500$ Pa (5% PEG)] for all RGD concentrations was evaluated on C2C12 cells. The number of C2C12 cells attached (adhesion) to the hydrogel surface was independent of the matrix stiffness and only influenced by the RGD concentration (Fig. S2b, ESI†). Interestingly, matrix stiffness influenced cellular spreading, with maximum spreading observed at *ca.* 250 Pa (2% PEG) (Fig. S2c, ESI†).

The influence of the matrix formulation in terms of stiffness and susceptibility towards degradation by matrix metalloproteases

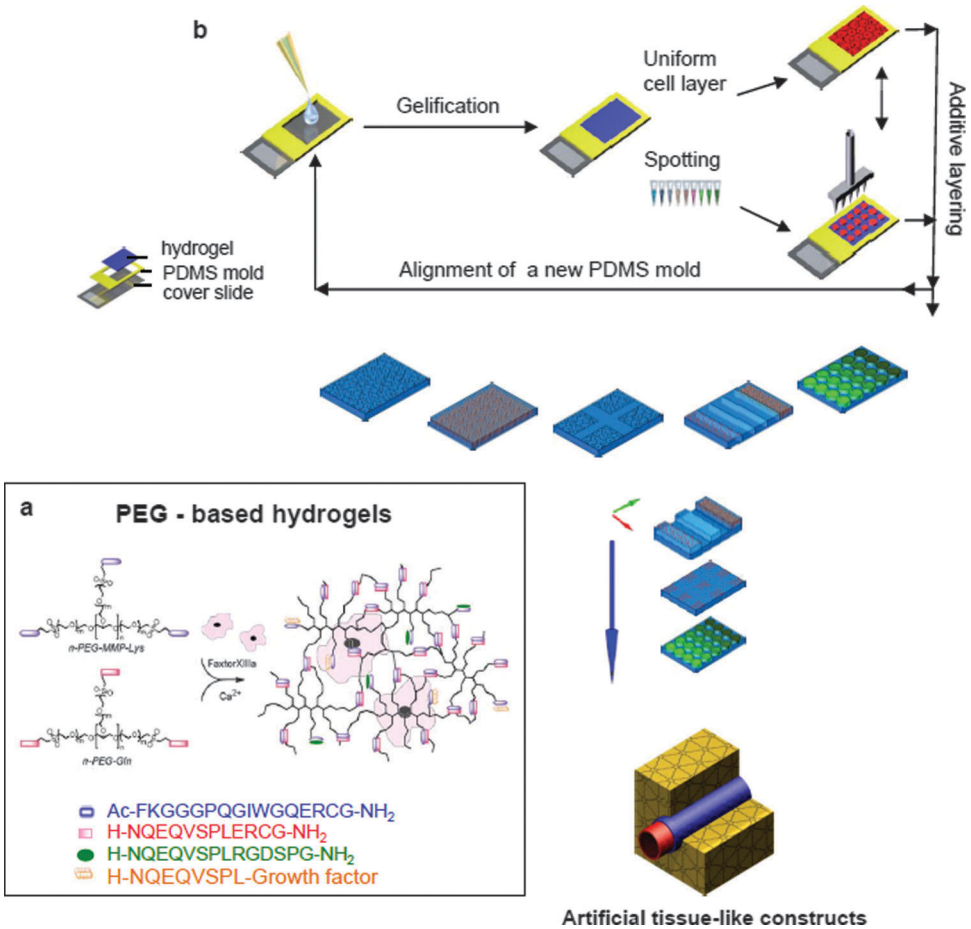

Fig. 1 Scheme of the artificial tissue-like construct formation. (a) Scheme of the synthetic artificial extracellular matrix system (aECM). (b) Presentation of the fabrication procedure. A first layer of modular designed PEG-based hydrogel is casted with the help of a PDMS mask, then combinations of cells, molecules, and hydrogels are deposited as either uniform or patterned layers. By repetitive alignment of PDMS molds and deposition of new layers, constructs with different heterogeneous designs are formed. Layer-by-layer assembly of individually patterned layers results in a tissue-like construct.

(MMPs) on 3D cellular spreading was evaluated on MC3T3-E1 cells encapsulated as single dispersed cells in FITC-labeled PEG gels that contained 50 μM RGD. As observed in confocal images with inverted FITC channels (showing matrix defects in green, Fig. 2a and c), cells in MMP-sensitive gels of intermediate stiffness (2%), within one day, migrate and leave behind tracks where the matrix has been remodelled. Nevertheless, in stiff MMP-sensitive gels (2.5%, $G' \approx 450$ Pa) cells are only spreading (Fig. 2e and g). In the MMP-insensitive intermediate stiffness gels (2%), where proteolytic migration is not possible, the cross-linking density of the matrix permits formation of filopodia but not cell migration in a proteolysis independent manner (Fig. 2b and d). By increasing the density of the MMP-insensitive matrix (2.5%) cells are even more restricted in their ability to form extensions (Fig. 2f and h). In addition, when MC3T3-E1 cells were entrapped in very stiff hydrogels (5%; $G' \approx 1.500$ Pa), cells were unable to elongate and, after 3 days in culture, stained positive for the membrane-impermeable ethidium homodimer (Fig. 2j *vs.* 2i). Such results are supported by previous findings.[38]

Taken together, these data indicate that survival and spreading of cells can be efficiently blocked by stiff matrices formulated with more than 2.5% PEG, by the absence of a MMP-degradable substrate, and by the lack of RGD. Therefore, such formulations could, in principle, be employed to engineer a microenvironment with defined barriers to prevent cells from trafficking from one gel area to another and to direct cellular spreading. From now on we will refer to them as non-permissive substrates.

Engineering of structured 3D constructs

Hierarchical structures with controlled 3D spatial organization of cells, matrix components, and biological cues were constructed by combining hydrogel engineering, robotic printing technology and layer-by-layer patterning. As illustrated in the depiction of the experiment (Fig. 1b), a layer of hydrogel ($2 \times 2 \times 0.2$ mm) was first cast with the help of a PDMS mask onto a glass slide and combinations of cells, molecules and hydrogels were deposited on the surface as either uniform or patterned films. Subsequently, the cycle consisting of alignment of a PDMS mold followed by the deposition of a new hydrogel layer was repeated multiple times to form a multi-layered structure. By defining the thickness of each PDMS mold (which can be varied from a few micrometres to hundreds of micrometres), the patterns of the matrix, the cellular components

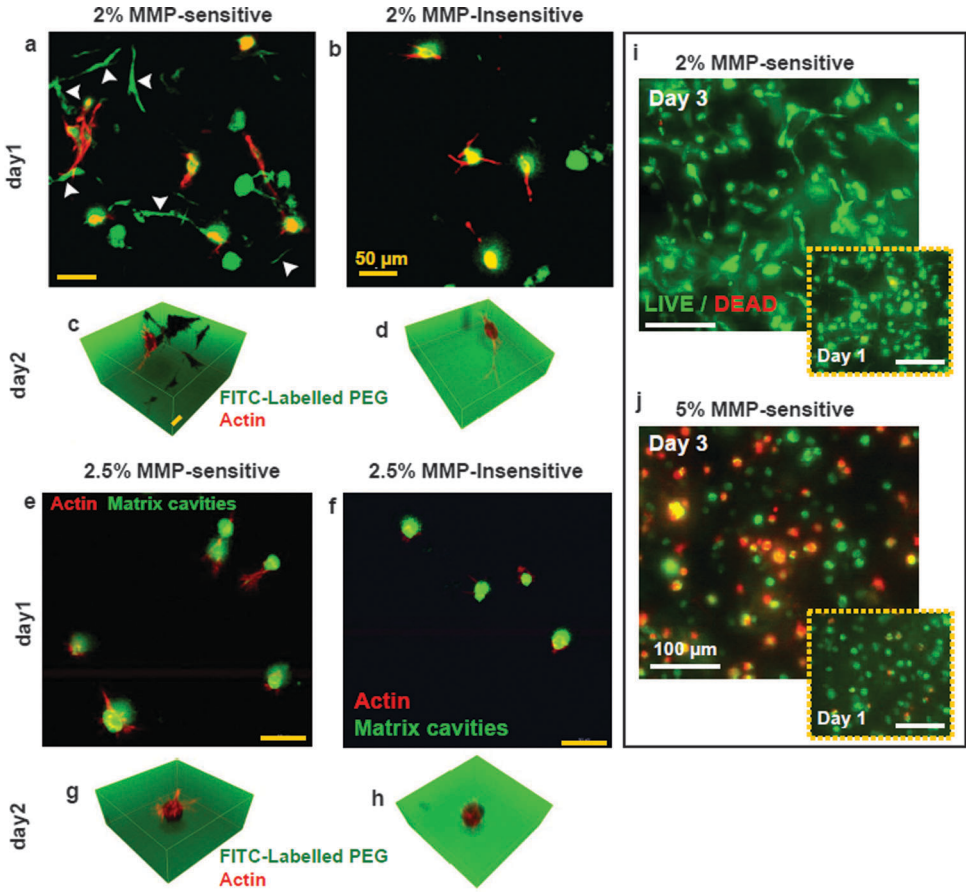

Fig. 2 Matrix stiffness and MMPs-susceptibility controlled 3D cell spreading and survival. (a–b, e–f) Projected confocal *z*-stacks (10×) of single MC3T3-E1 cells encapsulated in intermediate (2%) and stiff (2.5%) FITC-labeled hydrogels. The green channel was inverted to visualize cracks present in the matrix (in green and indicated with arrows in (a)). (c–d, g–h) 3D reconstructions of *z*-stacks at higher magnification (63×). (i, j) Cell survival of MC3T3-E1 cells encapsulated in 3D PEG gels of different stiffnesses by a live/dead assay. All together, these data show the dramatic influence of the matrix properties on the cells which have to overcome the physical barrier to be able to migrate within the 3D PEG matrix.

(independently for each layer) as well as the number of additive layers, any desired construct can be obtained.

We first tested the feasibility of the layer-by-layer approach by integrating homogeneous layers of cells and gel matrices. The reconstructed confocal image (Fig. 3a) shows a *z*-arrangement of confluent monolayers of C2C12 cells and laminated blocks of approximately 200-µm-thick hydrogels containing either labeled molecules (5% PEG, 50 µM Lys-FITC) or single dispersed cells (2.5% PEG, 50 µM Lys-RGD). Since gel layers can be formed in the presence of cells or can be used as surfaces for the seeding of cells, such a simple layering approach allows for a large variety of cell and matrix combinations. Next, to increase heterogeneity within each gel layer, we explored robotic printing platforms using a contact-spot arraying technology with a lateral precision of approximately 5 µm (Fig. 3b and c) and robotic pipetting with a lateral precision of approximately 100 µm (Fig. S3, ESI†). As exemplified with FITC- and Alexa-530-labeled peptides, spatially segregated hydrogel drops of *ca.* 100 µm diameter and 20 µm height (Fig. 3b and c) were formed on hydrogel layers of *ca.* 200 µm by using spotted array technology [by using robotic pipetting workstation (Fig. S3, ESI†); depots of *ca.* 900 µm diameter]. The size of the droplets can be modified by adjusting different parameters (*e.g.* pin-head size, amount of dispensed liquid, repetitive printing steps). In addition, due to the modularity of the PEG hydrogel, the fluorescent-labeled ligands are covalently tethered to the substrate thereby preventing any cross-contamination between the different areas, as observed in the 360° rotating videos of the spotted arrays (Videos S1 and S2, ESI†).

Cellular viability and functionality within 3D assemblies

Once engineering feasibility was proven, we characterized cell viability and functionality within 3D assemblies. To test whether cells remained viable during the additive layering process, we evaluated the capacity of the mouse myoblastic cell line C2C12 to differentiate into osteoblastic cells upon stimulation with soluble recombinant human bone morphogenetic protein 2 (rhBMP-2). To confirm the differentiation towards an osteoblastic phenotype within the construct, the presence of bone specific alkaline phosphatase (ALP), a marker for osteogenic differentiation, was determined immunohistochemically (Fig. 3d). Indeed, the uniform red staining indicating ALP expression (cell nuclei in blue) after stimulation with rhBMP-2 for 7 days demonstrated that C2C12 cells retained the capacity to respond to a morphogenic signal.

Next, we optimized spotting conditions and evaluated the ability of cells to spread after spotting. Spotting is a process

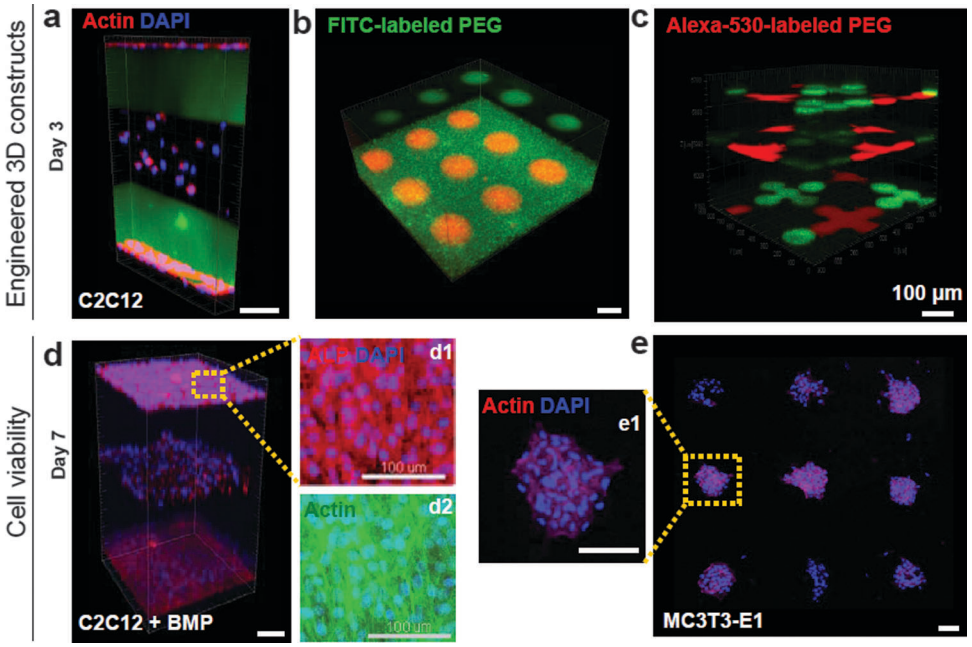

Fig. 3 Three-dimensional patterning of hydrogels. 3D constructs were analyzed by confocal microscopy and shown as reconstructed images. (a) Homogeneous layers of C2C12 cells and cell-containing or FITC-labeled gels (gel mass either in green or unstained). (b and c) Different fluorescently labeled hydrogels arranged by robotic printing in defined positions on top of different layers of hydrogel. (d) C2C12 retain their differentiation potential as demonstrated by staining of bone specific ALP expression after stimulation with BMP-2 for 7 days. (e) MC3T3-E1 cells spotted as single dispersed cells in 1% PEG spreaded within the droplets.

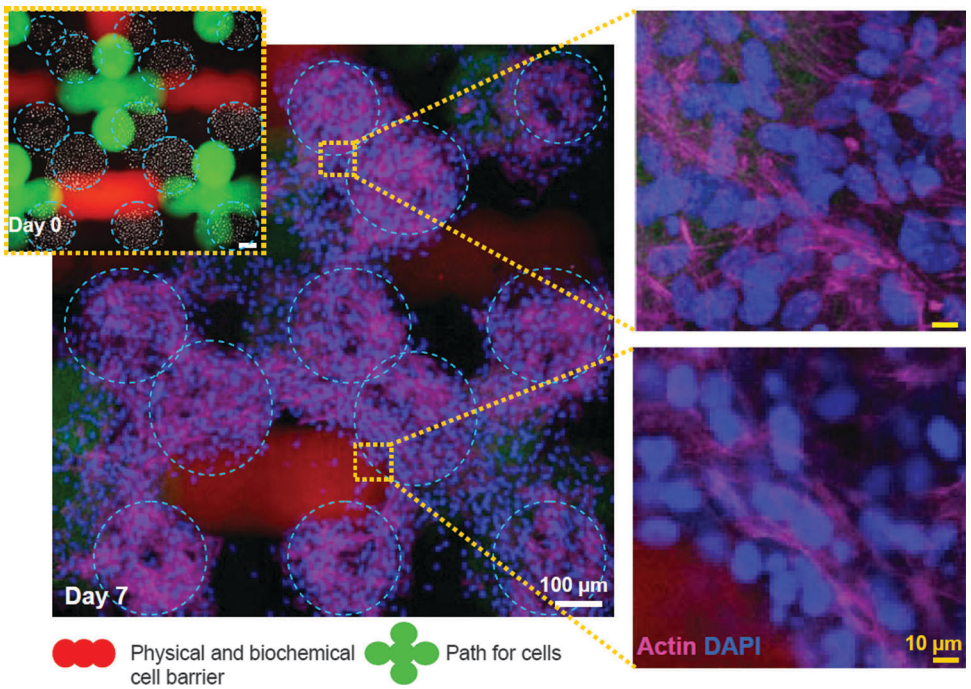

Fig. 4 Instructive PEG-based microenvironment to direct cellular spreading. Two formulations of hydrogels were spatially arranged to form regions that either permit (green) or act as barriers (red) for cell spreading. MC3T3-E1 cells were embedded in low density hydrogels and deposited in close contact to permissive and non-permissive regions. Subsequently the spotted experimental setup was further sandwiched within a non-permissive hydrogel mass. At day 0, MC3T3-E1 spots are delimited by circles. After 7 days in culture, cells spread within the permissive regions, while avoiding non-permissive hydrogels.

which, due to low volumes and thus relatively high evaporation of water, can induce changes in effective hydrogel precursor concentrations which may be critical for cell survival. In a series of experiments using different concentrations of PEG precursor, cell-friendly soft hydrogels were found to be formed starting from 1% initial PEG precursor content (data not

shown). Based on these findings, MC3T3-E1 cells were spotted as single dispersed cells in 1% PEG hydrogels containing 50 μM Lys-RGD. To restrict spreading to the site of deposition, the cell-matrix spots were embedded in non-permissive hydrogels. Cell spreading within the spotted areas (phalloidin in red) clearly indicated that cellular functions after the spotting procedure remained intact (Fig. 3e and Fig. S3, ESI†).

Directing cellular spreading by heterogeneous patterning

Based on our matrix engineering and patterning results, we rationally designed an instructive microenvironment which has the ability to direct and control cell migration. MC3T3-E1 cells were embedded in low density gels and spotted in close contact to spatially arranged formulations of hydrogels that were either permissive or resistant to cell migration (as previously defined). The green regions (Fig. 4) corresponded to cell-permissive hydrogels which contained 50 μM RGD and a cell-friendly PEG concentration (1%), whereas the non-permissive gels, stained in red, were formulated without RGD and with cross-linking densities (3%) that were impenetrable to cells. To prevent the escape of cells from the patterned areas this experimental setup was further embedded within a non-permissive hydrogel mass. The ability of PEG-based micro-environments to direct cellular behavior by mechanical and biological means was assessed by allowing cells to grow, proliferate, and spread in the patterned substrates for one week, under standard culture conditions. CLSM images revealed that the cells selectively spread into the migration-permissive paths and respected the imposed physiochemical barriers.

Artificial structured 3D tissue-like construct

To demonstrate the feasibility of creating 3D structured artificial tissue-like models by the assembly of instructive microenvironments, we aimed at engineering a well-defined and spatially organized bone tissue-like construct containing three constitutive bone cells: osteoblasts (MC3T3-E1), endothelial cells (HUVEC) and osteocytes (MLO) (Fig. 7a). One of the main limitations in tissue engineering is to engineer functional and vascularized tissues. This issue is particularly critical in tissue engineering approaches that involve pre-seeding of cells on a biomaterial scaffold. Furthermore, the development and healing of bone tissues *in vivo* is intimately regulated by the formation of a vascular network. Therefore, we targeted culture conditions that could support osteogenic differentiation of MC3T3-E1, and focused our evaluations on the ability of the endothelial cells to form a primitive vasculature-like structure.

We first addressed the medium composition of individual 2D cell mono-cultures to determine favorable culture conditions for later co-culture experiments in 3D. As expected, survival and morphology of all cell types were influenced by the medium composition. Interestingly, MC3T3-E1 cells (as well as C2C12 cells, data not shown) in HUVEC medium exhibited morphological changes and a significantly reduced osteogenic differentiation potential, as shown by impaired induction of ALP activity in response to rhBMP-2 treatment (Fig. 5a and Fig. S4, ESI†). A combination of 4 parts of MC3T3-E1 and 1 part of basal HUVEC medium did not affect cell morphology but slightly reduced the rhBMP-2 mediated increase of ALP activity (Fig. 5a and Fig. S4, ESI†). These data are consistent with the reported observation that complete endothelial medium is not sufficient to support the differentiation of C2C12 cells to muscle cells.[39] We defined the standard culture medium conditions based on morphological appearance, best survival and proliferation behavior of all cells as well as differentiation potential of MC3T3-E1 cells; 4 parts of MEM-α medium and 1 part of endothelial cell growth medium w/o supplements (BECM). This condition was subsequently tested in 3D monocultures.

MC3T3-E1 cells as well as MLO cells embedded in 3D PEG matrices (50 μM Lys-RGD) grow well and spread normally under such culture conditions (Fig. 5b). HUVEC monocultures under the same conditions (as well as in a standard HUVEC medium) adapted an elongated morphology and were active within the first days of culture. However, they did not form aggregates and their viability became compromised in the long-term (*ca.* ≤50% viability at day 7) (Fig. 5c).

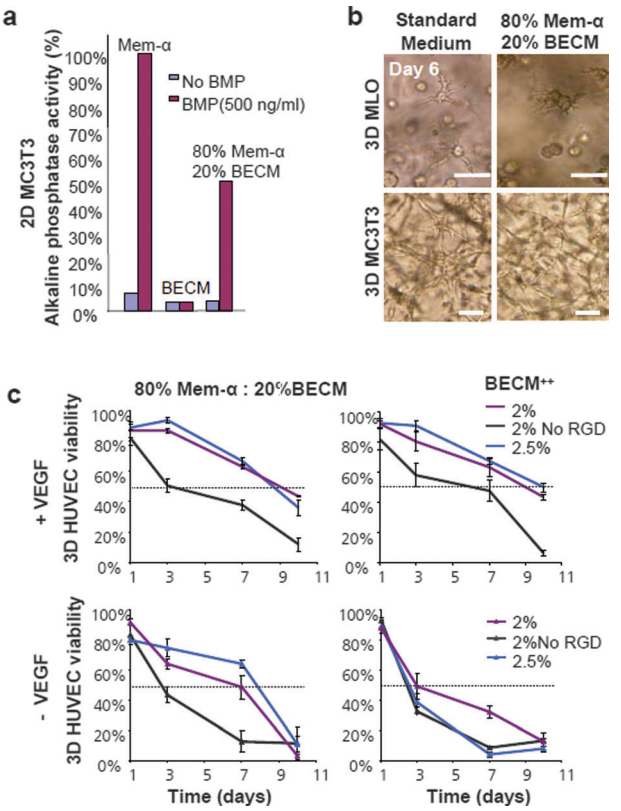

Fig. 5 Establishment of 3D culture conditions for MC3T3-E1, MLO and HUVEC mono-cultures. (a) Correlation between osteogenic differentiation and medium culture conditions. Alkaline phosphatase activity of MC3T3-E1 cells in the presence or in the absence of rhBMP-2 for selected medium compositions determined in 2D cultures. (b) Bright field images of 3D MC3T3-E1 and MLO mono-cultures in selected medium compositions. (c) Survival of HUVECs in PEG gels in the presence and absence of RGD and VEGF in two medium compositions. None of the tested conditions supported HUVEC survival over long periods of time (all conditions; day 10, viability ≤ 50%). Basal endothelial cell growth medium without supplements (BECM). BECM^{++} with supplements (standard medium).

The presence of RGD and the addition of 100 ng ml^{-1} soluble VEGF to the culture medium improved the viability of the cells over time. However, viability was less than 50% after 10 days in culture and cells did not aggregate nor form tube-like structures. These observations, in agreement with earlier reports,[40–42] suggest that in a microenvironment consisting of PEG matrix, RGD, endothelial medium, and soluble VEGF, single dispersed HUVECs cannot survive over long periods of time and cannot form a capillary network.

When co-cultures of single dispersed HUVEC and MLO or MC3T3-E1 cells were established in the presence of the integrin-binding ligand (RGD) and VEGF, a significant number of tube-like aggregates were found in the presence of MC3T3-E1 cells (Fig. 6). Interestingly, a large increase in the number of tubular structures was observed in the tri-culture system (HUVECs, MC3T3-E1, MLO cells) in the presence of both RGD and VEGF (Fig. 6). Stromal cells have been reported in earlier studies to be critical and sufficient for the induction of endothelial tubular structures in biologically derived matrices such as collagen, fibrin or matrigel.[39] Since such materials might contain many inherent biological signals, we assume that besides the supplementation of appropriate matrix domains, cell–cell communication might become even more critical for the morphogenesis of vascular structures in fully defined engineered biomaterials. In support of this, recently published data indicate that fully synthetic PEG-based matrices, in contrast to the biological counterparts fibrin or collagen, failed to support the attachment of HUVECs for longer than 3 days in culture. When TGFβ-4 was added to the same PEG system a vascular-like network formation after 12 hours was reported in 2D cultures, but not in 3D.[40]

Finally, once the culture conditions were defined, we assembled the three cell types in a well-controlled synthetic microenvironment to create spatially organized vascularized bone tissue-like constructs (Fig. 7b). Constructs were formed on a supportive layer of 4% PEG hydrogel covered with a monolayer of MC3T3-E1. Above this layer, HUVECs were subsequently positioned in 1 μl-sized hydrolytically and proteolytically degradable PEG-acrylate gels. These rapidly degradable PEG-acrylates were formed in the absence of Lys-RGD to prevent high concentrations of soluble RGD peptides which could potentially interfere with HUVEC viability. Immediately after gelation, a covering layer of 1.5% PEG containing human osteocytes was added. These assemblies were allowed to undergo morphogenetic remodeling for 10 days under the previously optimized medium conditions in the presence of 100 ng ml^{-1} soluble VEGF. After fixation, cell nuclei (DAPI/blue), cytoskeleton (phalloidin/green) and endothelial specific epitopes CD31 (red) were stained and evaluated by CLSM. Three-dimensional reconstructions of the *z*-stacks revealed a dense and interconnected network of CD31 positive cells where the HUVEC cells were deposited (Fig. 7c–e). At high magnification, CD31 negative cells which were likely to be osteoblastic cells were observed surrounding the endothelial structures (Fig. 7f).

In this section, we have provided evidence for the importance of the individual components involved in the efficient formation of vessel-like structures in artificial environments. By varying individual parameters of the system, we have defined an instructive *in vitro* microenvironment that promotes HUVEC re-assembly into tube-like structures in the context of bone. In this artificial milieu the presence of the adhesive

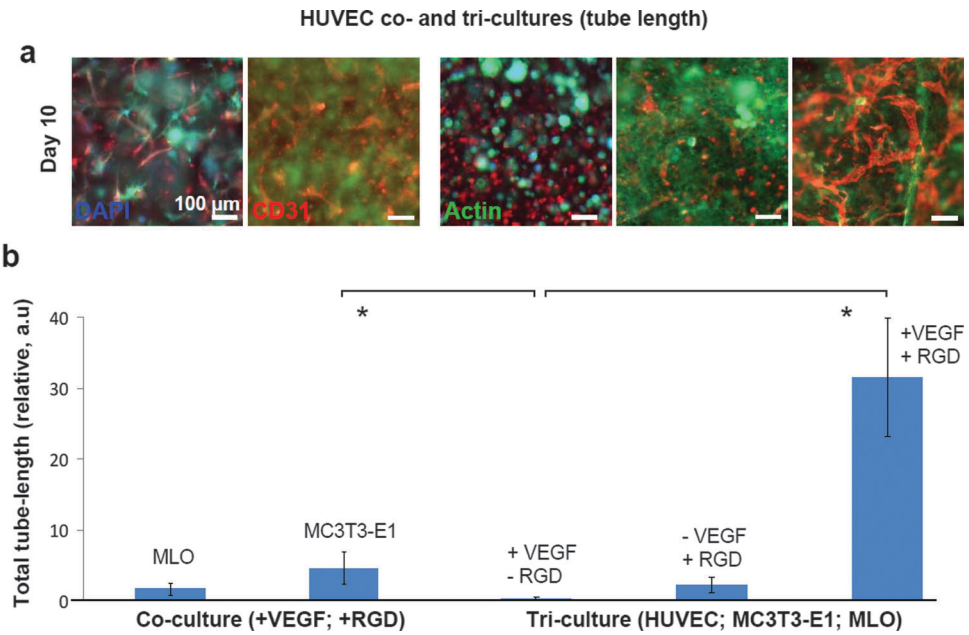

Fig. 6 Contribution of MC3T3-E1 and MLO to HUVEC vessel formation. (a) Fluorescence images showing the ability of HUVECs to form tubular-like structures under different microenvironmental compositions. (b) The influence of MC3T3-E1 and MLO cells, RGD and VEGF on HUVEC vessel formation was quantified by measuring total tubule-length in a series of combinatorial microenvironments. Only in the presence (minimum) of MC3T3-E1, VEGF and the integrin-binding ligand (RGD) did HUVECs reassemble to for capillary-like networks. Statistical significance analysis; Dunn' test ($n \geq 3$).

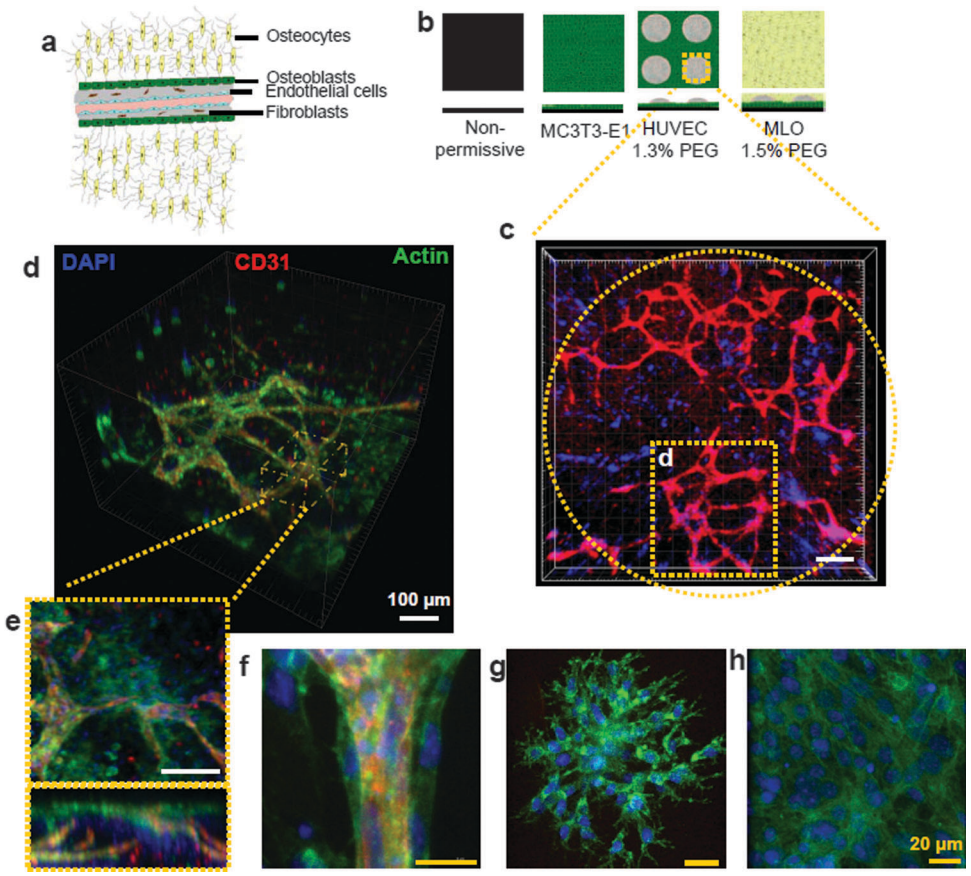

Fig. 7 Artificial bone tissue-like construct by assembly of an instructive microenvironment. (a) Schematic cartoon of bone. (b) Illustration of the assembly procedure to form a bone-like construct. (c–h) Confocal images of bone tissue-like assemblies allowed to remodel for 10 days under optimized co-culture condition. (c–e) Monolayer of MC3T3-E1 at the bottom. HUVECs assembled into tube-like structures within the PEG droplets in the middle of the construct. Aggregates or single dispersed MLOs at the top. High resolution images (63×) of (f) the capillary-like network, (g) MLO and (h) MC3T3-E1 cells. 3D sampling reconstruction was performed by Imaris software.

ligand RGD, adequate stromal cells and the angiogenic growth factor VEGF were necessary to support the long term survival of endothelial cells and the induction of capillary-like tube formation. Furthermore we have been able to engineer a 3D spatially organized vascularized bone tissue-like construct by the assembly of instructive microenvironments.

The exact role of either preosteoblastic cells or osteocytes on endothelial cell function is still unclear. However, recent data have indicated that endothelial cells may secrete prostaglandins and thereby stimulate osteoblasts to provide VEGF and produce collagen type I. Indeed gene profiling and immunohistochemical evaluations suggested that matrix components such as collagen type I might act as a matrix cue to give direction and allow adhesion of a forming vascular structure.[43] Osteocytes are also known to play an important role in cross-talk with other cells; indeed, they have been shown to secrete important signaling molecules such as prostaglandin, nitric oxide, glutamate, sclerostin and insulin-like GF.[44–46] It is therefore likely that in our culture system, MLO cells (in response to the tri-culture condition) secret signaling molecules that enhance communication between OBs and ECs or directly promote the ability of HUVEC cells to form tube-like structures. However, at this stage we do not know the molecular mechanisms that control the arrangement of the different cell types. Further evaluation of the influence of MC3T3-E1 and MLO cells on the bone tissue-like assembly, as well as the determination of the presence of lumen and matrix depositions by MC3T3-E1 are the subjects of ongoing work. Interestingly, the phenotype of the stromal cells has been reported to be critical for the induction of tubular structures in endothelial cells. For example, endothelial cells embedded in matrigel formed tubular structures in co-cultures with C2C12 in a sponge-like material consisting of 50% poly(L-lactic acid) (PLLA) and 50% polylactic-glycol acid (PLGA). However, the addition of embryonic fibroblast resulted in an increased expression of VEGF and in more extended vascular structures.[39]

Conclusions

Based on the widely accepted theory that natural structured microenvironments surrounding cells are critical for tissue formation, homeostasis and regeneration, we present a controllable and reliable platform to generate 3D organized instructive microenvironments. We exploit synthetic aECM matrices that can be formed in the presence of cells under physiological conditions by an enzyme-mediated reaction. Such systems can be engineered towards their mechanical

properties and biological activity upon a passive background. The combination of these aECM with patterning and layering approaches allows for the recapitulation of spatially heterogeneous environments (matrix components, biological cues, and cells) that mimic many aspects of the natural situation. Such spatially-defined microenvironments may be necessary to initiate and guide the formation of artificial tissues *in vitro*. Indeed, the formation of hierarchically ordered and functional tissues during development and their eventual repair in later life is directed by highly orchestrated processes. Recapitulating these processes *in vitro* will largely depend on our capacity to understand, control and mimic such signaling networks.

A better understanding of the mechanisms governing morphological, physiological and pathophysiological processes *in vitro* will translate into the development of novel clinical therapies that prevent or cure underlying diseases. Here, by showing the feasibility of simultaneous patterning of matrix components, ligands, and cells to direct cellular spreading and to form artificial tissue-like constructs, we introduce a general method to create organized artificial instructive microenvironments. Such a platform allows for the dissection of biological questions related to tissue remodeling and morphogenesis, and their independent study in a fully controllable artificial environment. Further understanding and automation of the procedure could lead to large scale production of for example reproducible tissue-like constructs suitable for high throughput screening.

Acknowledgements

We want to thank Prof. L. Bonewald (University of Missouri—Kansas City) and the University of Texas Health Science at San Antonio to provide us with the osteocyte-like MLO cells. This work was supported by the Competence Centre for Materials Science and Technology and "Angioscaff".

Notes and references

1 P. G. Campbell and L. E. Weiss, *Expert Opin. Biol. Ther.*, 2007, **7**, 1123.
2 D. L. Kaplan, R. T. Moon and G. Vunjak-Novakovic, *Nat. Biotechnol.*, 2005, **23**, 1237.
3 S. R. Khetani and S. N. Bhatia, *Curr. Opin. Biotechnol.*, 2006, **17**, 524.
4 E. S. Place, N. D. Evans and M. M. Stevens, *Nat. Mater.*, 2009, **8**, 457.
5 N. Huebsch and D. J. Mooney, *Nature*, 2009, **462**, 426.
6 L. G. Griffith and M. Swartz, *Nat. Rev. Mol. Cell Biol.*, 2006, **7**, 211.
7 F. Rosso, A. Giordano, M. Barbarisi and A. J. Barbarisi, *Cell. Physiol.*, 2004, **199**, 174.
8 W. P. Daley, S. B. Peters and M. J. Larsen, *Cell Sci.*, 2008, **121**, 255.
9 R. O. Hynes, *Science*, 2009, **326**, 1216.
10 M. Votteler, P. J. Kluger, H. Walles and K. Schenke-Layland, *Macromol. Biosci.*, 2010, **10**, 1302.
11 M. P. Lutolf and J. A. Hubbell, *Nat. Biotechnol.*, 2005, **23**, 47.
12 M. P. Lutolf, *Integr. Biol.*, 2009, **1**, 239.
13 M. W. Tibbitt and K. S. Anseth, *Biotechnol. Bioeng.*, 2009, **103**, 655.
14 M. Ehrbar, S. C. Rizzi, R. G. Schoenmakers, B. San Miguel, J. A. Hubbell, F. E. Weber and M. P. Lutolf, *Biomacromolecules*, 2007, **8**, 3000.
15 M. Ehrbar, S. C. Rizzi, R. Hluschchuk, V. Djonov, A. H. Zisch, J. A. Hubbell, F. E. Weber and M. P. Lutolf, *Biomaterials*, 2007, **28**, 3856.
16 M. P. Lutolf and J. A. Hubbell, *Biomacromolecules*, 2003, **4**, 713.
17 T. P. Kraehenbuehl, L. S. Ferreira, P. Zammaretti, J. A. Hubbell and R. Langer, *Biomaterials*, 2009, **30**, 4318.
18 S. A. DeLong, J. J. Moon and J. L. West, *Biomaterials*, 2005, **26**, 3227.
19 C. A. DeForest, B. D. Polizzotti and K. S. Anseth, *Nat. Mater.*, 2009, **8**, 659.
20 J. H. Wosnick and M. S. Shoichet, *Chem. Mater.*, 2008, **20**, 55.
21 A. M. Kloxin, A. M. Kasko, C. N. Salineas and K. S. Anseth, *Science*, 2009, **324**, 59.
22 V. Mironov, T. Boland, T. Trusk, G. Forgacs and R. R. Markawald, *Trends Biotechnol.*, 2003, **21**, 157.
23 W. C. J. Wilson and T. W. Boland, *Anat. Rec., Part A*, 2003, **272**, 491.
24 T. Boland, V. Mironov, A. Gutowska, E. A. Roth and R. R. Markwald, *Anat. Rec., Part A*, 2003, **272**, 497.
25 T. Xu, J. Joyce, C. Gregory, J. J. Hickman and T. Boland, *Biomaterials*, 2005, **26**, 93.
26 C. Y. Chen, J. A. Barron and B. R. Ringeisen, *Appl. Surf. Sci.*, 2006, **252**, 8641.
27 D. R. Albrecht, U. H. Gregory, T. B. Wassermann, R. L. Sah and S. N. Bhatia, *Nat. Methods*, 2006, **3**, 369.
28 Z. Nie and E. Kumacheva, *Nat. Mater.*, 2008, **7**, 277.
29 R. Sudo, S. Chung, I. K. Zervantonakis, V. Vickerman, Y. Toshimitu, L. G. Griffith and R. D. Kamm, *FASEB J.*, 2009, **23**, 1.
30 A. Folch and M. Toner, *Annu. Rev. Biomed. Eng.*, 2000, **2**, 227.
31 M. L. Yarmush and K. R. King, *Annu. Rev. Biomed. Eng.*, 2009, **11**, 235.
32 D. J. Odde and M. J. Renn, *Biotechnol. Bioeng.*, 1999, **67**, 312.
33 Y. K. Nahmias and D. J. Odde, *Nat. Protoc.*, 2006, **1**, 2288.
34 V. L. Tsang, A. A. Chen, L. M. Cho, K. D. Jadin, R. L. Sah, S. DeLong, J. L. West and S. N. Bhatia, *FASEB J.*, 2007, **21**, 790.
35 A. Ichinose, T. Tamaki and N. Aoki, *FEBS Lett.*, 1983, **153**, 369.
36 B. H. Hu and P. B. Messersmith, *J. Am. Chem. Soc.*, 2003, **125**, 14298.
37 A. Sala, M. Ehrbar, D. Trentin, R. G. Schoenmakers, J. Vörös and F. E. Weber, *Langmuir*, 2010, **26**, 11127.
38 M. Ehrbar, A. Sala, P. Lienemann, A. Ranga, K. Mosiewicz, A. Bittermann, S. C. Rizzi, F. E. Weber and M. P. Lutolf, *Biophys. J.*, 2011, **100**, 284.
39 S. Levenberg, J. Rouwkema, M. Macdonald, E. S. Garfein, D. S. Kohane, D. C. Darland, R. Marini, C. A. van Blitterswijk, R. C. Mulligan, P. A D'Amore and R. Langer, *Nat. Biotechnol.*, 2005, **23**, 879.
40 D. Seliktar, A. H. Zisch, M. P. Lutolf, J. L. Wrana and J. A. Hubbell, *J. Biomed. Mater. Res., Part A*, 2004, **68**, 704.
41 J. E. Leslie-Barbick, J. J. Moon and J. L. West, *J. Biomater. Sci., Polym. Ed.*, 2009, **20**, 1763.
42 T. P. Kraehenbuehl, L. S. Ferreira, P. Zammaretti, J. A. Hubbell and R. Langer, *Biomaterials*, 2009, **30**, 4318.
43 M. I. Santos, R. E. Unger, R. A. Sousa, R. L. Reis and C. J. Kirkpatrick, *Biomaterials*, 2009, **30**, 4407.
44 B. S. Noble and J. Reeve, *Mol. Cell. Endocrinol.*, 2000, **159**, 7.
45 L. Bonewald, *J. Musculoskeletal Neuronal Interact.*, 2006, **6**, 331.
46 L. Bonewald, *Ann. N. Y. Acad. Sci.*, 2007, **1116**, 280.